

1 An end-to-end approach for protein folding by integrating 2 Cryo-EM maps and sequence evolution

3
4 Pan Li^{1,2}, Liangyue Guo^{1,2}, Haibin Liu^{1,2}, Binghua Liu¹, Fanhao Meng¹, Xiaodan Ni¹, Allen Chunlong
5 Guo^{1*}

6
7 **Affiliations:**

8 ¹Shuimu BioSciences, Changping Life Science Park, Beijing 102206, China

9 ²These authors contributed equally: Pan Li, Liangyue Guo and Haibin Liu

10
11 *Correspondence: chunlong@shuimubio.com (C.G.)

12
13 **Abstract**

14 Protein structure modeling is an important but challenging task. Recent breakthroughs in Cryo-EM
15 technology have led to rapid accumulation of Cryo-EM density maps, which facilitate scientists to
16 determine protein structures but it remains time-consuming. Fortunately, artificial intelligence has
17 great potential in automating this process. In this study, we present SMARTFold, a deep learning
18 protein structure prediction model combining sequence alignment features and Cryo-EM density map
19 features. First, using density map, we sample representative points along the predicted high
20 confidence areas of protein backbone. Then we extract geometric features of these points and integrate
21 these features with sequence alignment features in our proposed protein folding model. Extensive
22 experiments confirm that our model performs best on both single-chain and multi-chain benchmark
23 dataset compared with state-of-the-art methods, which makes it a reliable tool for protein atomic
24 structure determination from Cryo-EM maps.

25
26 **Introduction**

27 Protein folding problem is one of the most fundamental problems in the field of biology. The way
28 proteins work and perform functions is largely determined by their unique three-dimensional
structures, so it is important to know the three-dimensional structure of a protein.

29 In recent years, cryo-electron microscopy (Cryo-EM) technology has made breakthrough progress
30 (Nakane et al., 2020; Yip et al., 2020). Cryo-EM electron density maps provides rich information of
31 protein structure and is of great help for structural modeling. Consequently, it has become a reliable
32 guidance for structural biologists to analyze protein structures. To expedite the Cryo-EM analyses,
33 many software tools have been developed for Cryo-EM data processing, such as RELION (Scheres,
34 2012) and CryoSPARC (Punjani et al., 2017). They use iterative optimization algorithms to estimate
35 the pose parameters for particles and reconstruct 3D map. CryoDRGN (Zhong et al., 2021) and
36 e2gmm (Chen and Ludtke, 2021) reconstruct multiple continuous conformations from single particle

37 dataset through deep learning. After density maps are produced, a critical step is to build the 3D
38 atomic model. Although a large number of related methods have been developed (He et al., 2022;
39 Jamali et al., 2022; Pfab et al., 2021; Terashi and Kihara, 2018; Terwilliger et al., 2018), automatic
40 model building from Cryo-EM density map remains as a time-consuming and labor-intensive job.

41 Meanwhile, with advancements in protein crystallography and cryo-electron microscopy, a large
42 amount of protein structures have been unveiled, which provides a good foundation for AI to study the
43 relationship between protein sequence and structure. In recent years, many scholars have devoted
44 themselves to using artificial intelligence algorithms to solve the problem of automatically predicting
45 3D atom positions from protein sequences (Baek et al., 2021; Jumper et al., 2021; Xu, 2019).

46 AlphaFold2 (Jumper et al., 2021) is a breakthrough in this field. Compared to previous research,
47 AlphaFold2, for the first time, realized end-to-end prediction from amino acid sequence to atomic
48 coordinates by integrating evolutional information from MSA, and achieved atomic-level accuracy
49 (The average prediction error is within 1 Angstrom in CASP14). Although AlphaFold2 has
50 outstanding performance, it is designed to predict 3D structures given protein sequence only.
51 Experimental information like EM density map is not used as input. Building structures solely from
52 sequence has two limitations. First, it does not utilize the essential experimental information of the
53 structure to be predicted, and highly relies on the result of MSA. Poor MSA search results could lead
54 to bad predictions; Moreover, it is very common that protein chains may have more than one
55 conformations, which means same chain sequence could have different 3D structures in different
56 environments, but AlphaFold2 always gives the same result for same sequence input.

57 Several researches have been done to automatically build structure from Cryo-EM maps. DeepTracer
58 (Pfab et al., 2021) is the first deep learning effort to build atom level structure from Cryo-EM density
59 maps. It treats the problem as an image segmentation task. It uses a U-Net model (Ronneberger et al.,
60 2015) to identify main chain atom positions from the density map, and then apply heuristic approach
61 to determine the atomic structure. A notable limitation is that it does not input protein sequence to the
62 model. Therefore, it relies on several post-processing steps after the segmentation model, including
63 tracing and alignment. These could lead to local fitting issues or tracing/connectivity problems.
64 Besides, experimental Cryo-EM maps could have noises and some regions like side chains are often
65 obscure, which makes it challenging to construct all-atom structure models if no sequence information
66 is given.

67 Similar prediction protocol is adopted in other methods, including EMBuild (He et al., 2022) .
68 ModelAngelo (Jamali et al., 2022), etc.. EMBuild begins by predicting main-chain probability maps
69 using a nested U-Net. Subsequently, it integrates AlphaFold2 structure prediction, FFT-based global
70 fitting, domain-based semi-flexible refinement, and graph-based iterative assembling with predicted
71 probability maps to construct structures. Its performance highly depends on the quality of AlphaFold2
72 prediction. It tends to give unsatisfactory results when AlphaFold2 is not accurate. ModelAngelo
73 (Jamali et al., 2022) starts with a CNN to initialize a graph representation with nodes assigned to
74 individual amino acids, and then refines the graph with a GNN, to combine Cryo-EM and sequence
75 information. Finally a hidden Markov model (HMM) is applied to post-process the graph to search the

76 mappings for each chain to entries in a user input sequence file. However, ModelAngelo is sensitive to
77 resolution. Its performance starts degrading at resolutions worse than 3.5Å.

78 In this work, we propose a novel approach, SMARTFold, to integrate cryo-EM density map with
79 sequence evolution for protein folding. This integration is achieved by sampling representative points
80 (“support points”) from the EM density map, and then use MSA together with these points as model
81 input. The foundational architecture of SMARTFold comes from AlphaFold2 and
82 AlphaFold-Multimer (Evans et al., 2022). Our key contributions are as follows:

83 1) we employ a U-Net to extract a representative point cloud, which captures backbone information
84 from the sparsely populated 3D EM density map. The geometric features of these points are utilized as
85 inputs for our model.;

86 2) we develop a novel module named EMformer to fuse the features from MSA and point cloud for
87 protein structure folding;

88 3) through our uniquely designed point-residue distogram head, the model can learn the relationship
89 between each support point and residue;

90 4) we introduce a distinctive feature termed “point-residue affinity” to mitigate the ambiguity problem
91 of homomultimer training.

92 Our model outputs full atomic structure prediction directly and no post processing steps are needed.
93 To the best of our knowledge, our approach is the first end-to-end deep learning model to learn
94 structure determination directly from both evolutional information and EM map features. Our
95 experiments show that SMARTFold outperforms methods used in previous studies on public protein
96 data.

97 **Results**

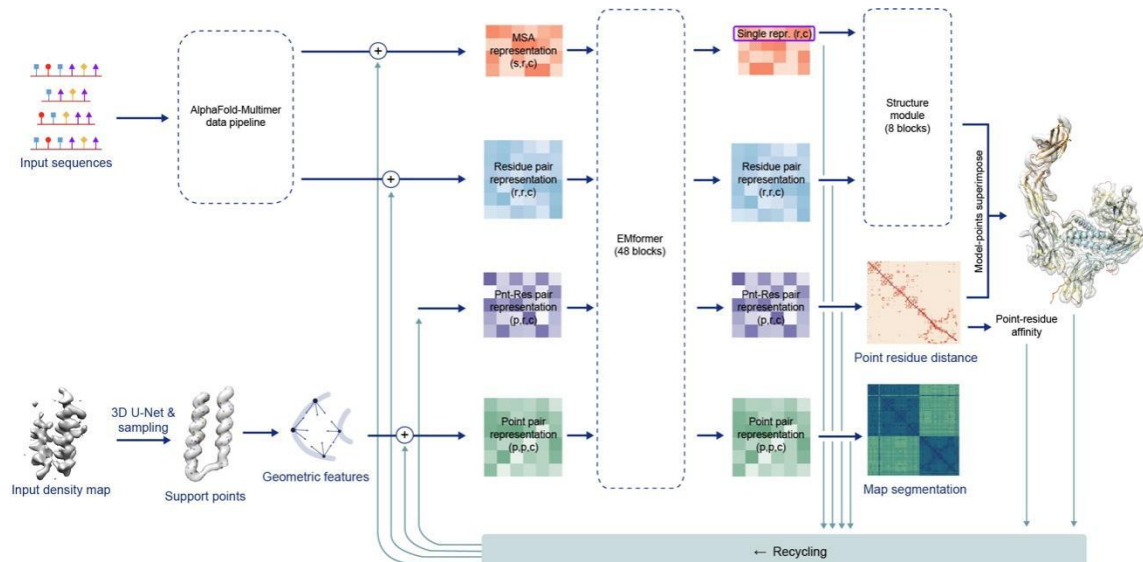
98 **Overview of SMARTFold**

99 The overall model of SMARTFold is inspired by recent advances in protein structure prediction with
100 deep neural networks used in AlphaFold2, except that the density map is also introduced as input (**Fig. 1**).
101 The input of SMARTFold includes the residue sequences and Cryo-EM density map. Similar to
102 AlphaFold2, we used the sequences to search MSA and PDB templates and fed these features into our
103 model (**SI 3.1**). To represent the density map, we first use a U-Net to identify backbone confidence
104 (Pfab et al., 2021), and then sample support points from the confidence map. The extracted geometric
105 features of support points are also fed into the model (**SI 2**). Next we develop a special embedding
106 module called EMformer, which is the most crucial part in our model, to combine the support point
107 features with sequence evolutional features (**SI 4**). Finally, a structure module same as the one in
108 AlphaFold2 is used for atomic structure prediction. A point residue distogram prediction head is used
109 to supervise point-residue relations in training and helps superimpose the predicted structure into
110 density map to get the final fitted structure (**SI 6.2**). Similar to AlphaFold2, the representations learned
111 after EMformer can be recycled to improve the model performance. To avoid the ambiguity of

112 homomultimer inference, the point-residue affinity can be inferred from point residue distogram to
113 match residues and points (**SI 7**).

114 The SMARTFold model was trained on 8,749 map/model pairs (see **SI 1** for dataset details) and the
115 parameters was initialized with AlphaFold2's parameters. Due to memory restriction, the sequence
116 features and support points are cropped to fragments containing a maximum of 320 amino acids. All
117 loss functions in AlphaFold2 are used in SMARTFold, with a slight change. These include the
118 weighted backbone FAPE loss, side chain FAPE loss, etc. (see **SI 6**). Corresponding to new added
119 heads, several new loss functions are introduced, including point-residue distogram loss, point
120 segmentation loss and point noise loss (see **SI 6**). All loss functions satisfy translation and rotation
121 invariance.

122



123

124 **Figure 1.** Model architecture of SMARTFold. There are two branches for model input: sequences (left
125 upper) and density map (left bottom). The input sequence is fed into the AlphaFold-Multimer data
126 pipeline to search for MSA sequences and PDB templates, and then initialize the MSA representation
127 and residue pair representation. Support points are sampled from the backbone confidence map, which
128 is inference by 3D U-Net from the raw density map. Geometric features of these support points are
129 embedded into point pair representation. A point-residue pair representation is introduced to maintain
130 the relationships between support points and residues. In EMformer, MSA representation, residue pair
131 representation, point-residue pair representation and point pair representation exchange their messages
132 and get updated. The first row of MSA representation (single representation) and the residue pair
133 representation are input to 8 consecutive structure module blocks to build 3D atomic model. A point
134 residue distogram head is built upon the updated point-residue pair representation to predict the
135 distance between each support point and residue. Highly confident “contact” point-residue
136 relationship can be used to fit the structure model into the raw EM density map. The four
137 representations above and the predicted C_β distogram (from 3D model) are fed to the next recycle to

138 promote the structure prediction.

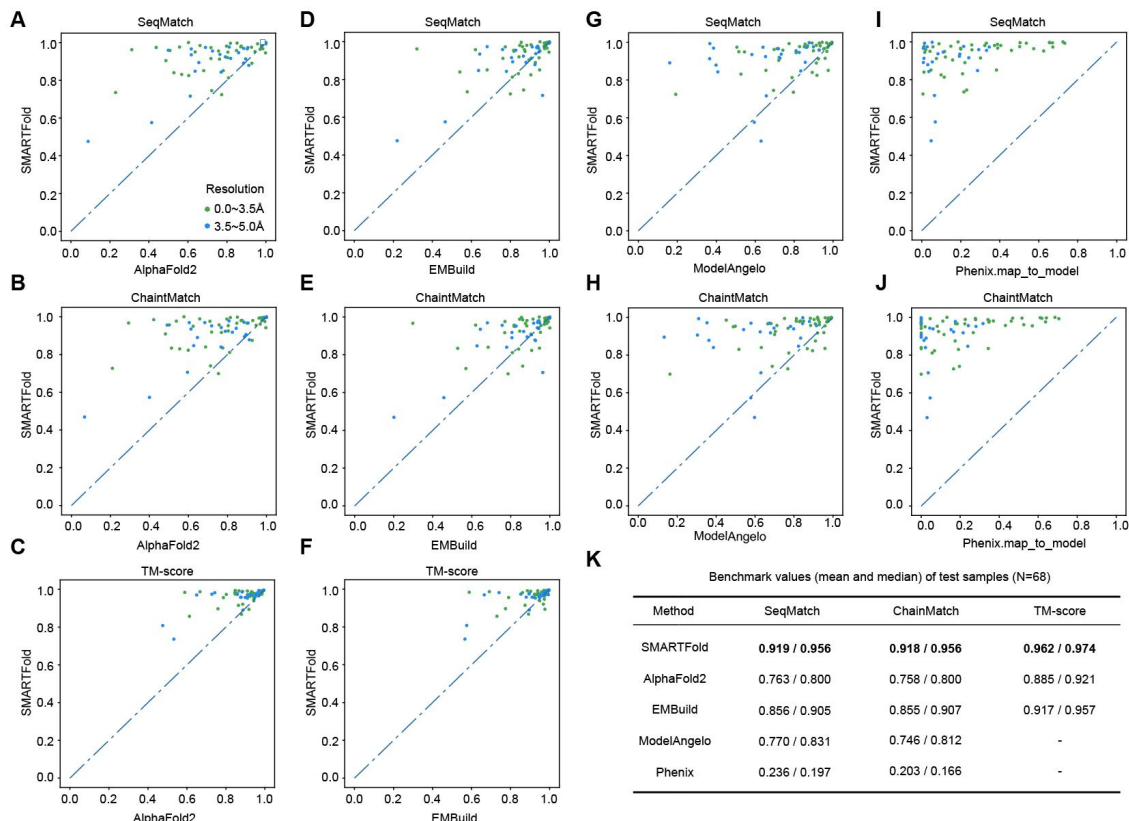
139 **Evaluating built models against the high-resolution single-chain dataset**

140 To compare the performance of SMARTFold with other methods and tools, we constructed four
141 representative benchmark datasets from testing set: high-resolution single-chain dataset,
142 high-resolution multiple-conformation single-chain dataset, high-resolution multi-chain dataset and
143 low-resolution dataset. For each dataset, duplicated samples were removed to ensure that the
144 maximum sequence similarity is less than 40% between each pair. Due to limited GPU memory, we
145 only kept those models with a total sequence length of less than 2500 for the benchmark evaluation.

146 We first evaluated our results on single-chain dataset. This is a subset of the benchmark dataset that
147 consists of 27 single-chain PDBs and 41 segmented PDB chains with resolution $\leq 5\text{\AA}$. We compared
148 our results against AlphaFold2 (Jumper et al., 2021), EMBuild (He et al., 2022), ModelAngelo (Jamali
149 et al., 2022), and Phenix.map_to_model (Terwilliger et al., 2018). We used SeqMatch, ChainMatch
150 and TM-score (Zhang and Skolnick, 2004) to evaluate the performance of each method. SeqMatch
151 measures the proportion of residues in the deposited model that are within 3\AA of the predicted amino
152 acid. On the basis of SeqMatch, ChainMatch further requires that the amino acid types of the upstream
153 and downstream adjacent residues for each position match those in the deposited model. TM-score
154 quantifies the topological similarity between two protein structures. All predicted structures were
155 aligned to deposited PDB structures using US-align (Zhang et al., 2022) before calculating metric
156 values.

157 **Fig. 2** illustrates the results of our model on single-chain data compared to other methods, and the
158 overall metrics is reported in **Fig. 2K**. It can be seen from **Fig. 2A-J** that for most test cases, our
159 model outperformed all the other methods listed (ChainMatch: 0.918 vs. 0.758, 0.855, 0.764 and
160 0.203). EMBuild is the second-ranked method. Since ModelAngelo and Phenix produce many
161 discontinuous and short segments, TM-score was not calculated for these two methods.

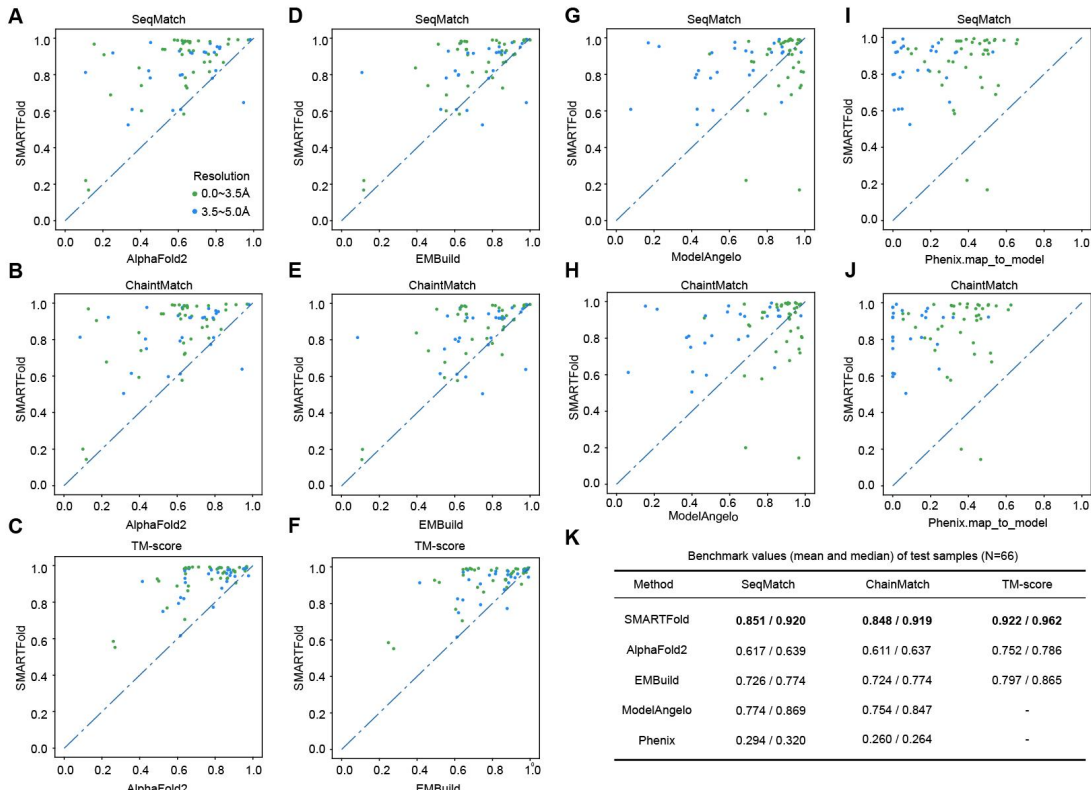
162



163

164 **Figure 2.** Comparison between SMARTFold, AlphaFold2, ModelAngelo and Phenix on 68
165 single-chain dataset.

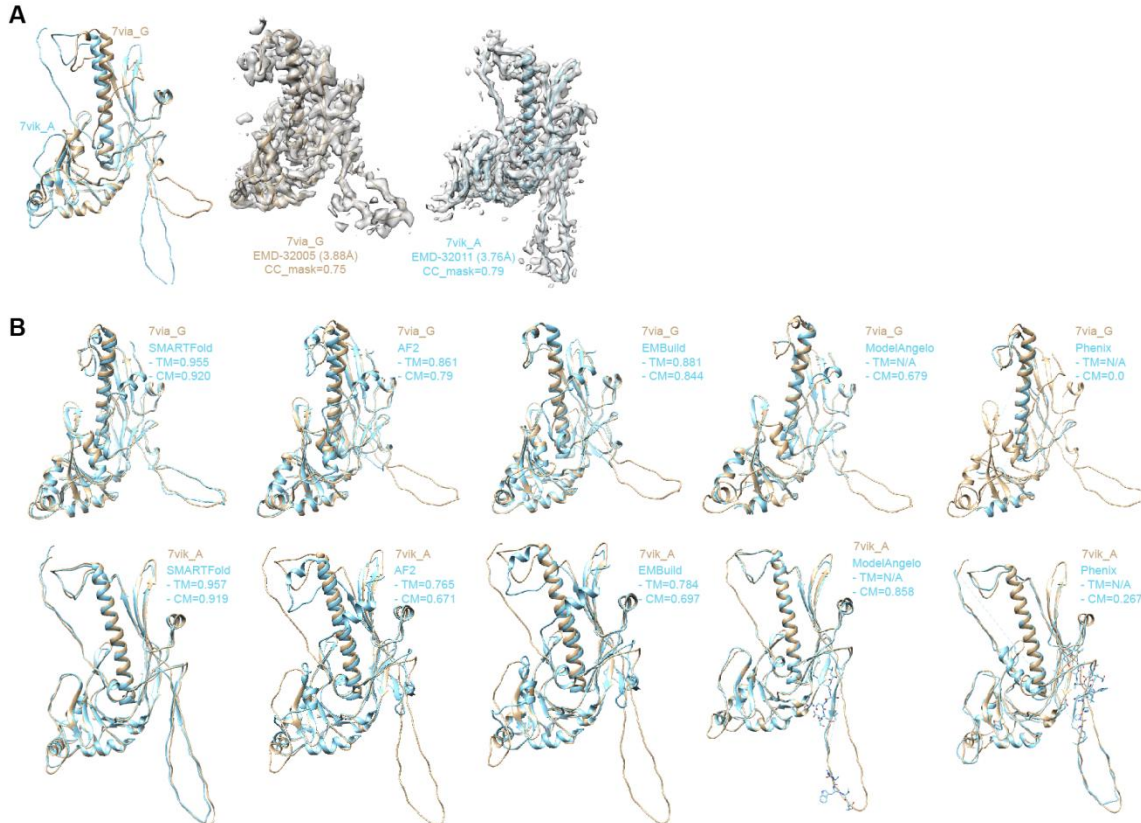
166 Compared with AlphaFold2, our method obtains structural information not only from MSA, but also
167 from support points. To prove that the support points can constrain the protein folding, we selected 28
168 groups of multi-conformational segmented PDB chains. Each group contains 2~8 PDB chains with
169 highly similar sequences (>90%) but very different structures (pairwise TM-score<0.8). This dataset
170 contains a total of 66 PDB chains with resolution ≤ 5 Å and has no intersection with the single-chain
171 dataset in **Fig. 2**. We compare our results against AlphaFold2, EMBuild, ModelAngelo, and Phenix
172 map_to_model (**Fig. 3**). It can be seen that our method is much better than others at predicting specific
173 protein conformations (ChainMatch: 0.848 vs. 0.611, 0.724, 0.754, 0.260). Given that sequences in
174 each group are highly similar, AlphaFold2 predictions highly resembled with each other within a
175 single group. Furthermore, since EMBuild relies on templates derived from AlphaFold2, it also gave
176 poor results in this case.



177

178 **Figure 3.** Comparison between SMARTFold, AlphaFold2, EMBuild, ModelAngelo and Phenix on 66
179 single-chain multi-conformational dataset.

180 **Fig. 4A** shows an example of bacteriophage lambda capsid protein (Wang et al., 2022). The same
181 sequence exhibits distinct structures in precursor capsid protein (procapsid, PDB: 7via_G) and mature
182 capsid protein (PDB: 7vik_A), with a pairwise TM-score of 0.770. The main difference between the
183 two structures lies in the loop region. The segmented Cryo-EM density maps fit well with the two
184 deposited structure models respectively (correlation coefficient values: 0.75 and 0.79). **Fig. 4B** shows
185 structural model from 5 methods on two density maps. Only SMARTFold successfully predicted the
186 correct loop structures for the two different conformations (**Fig. 4B**).

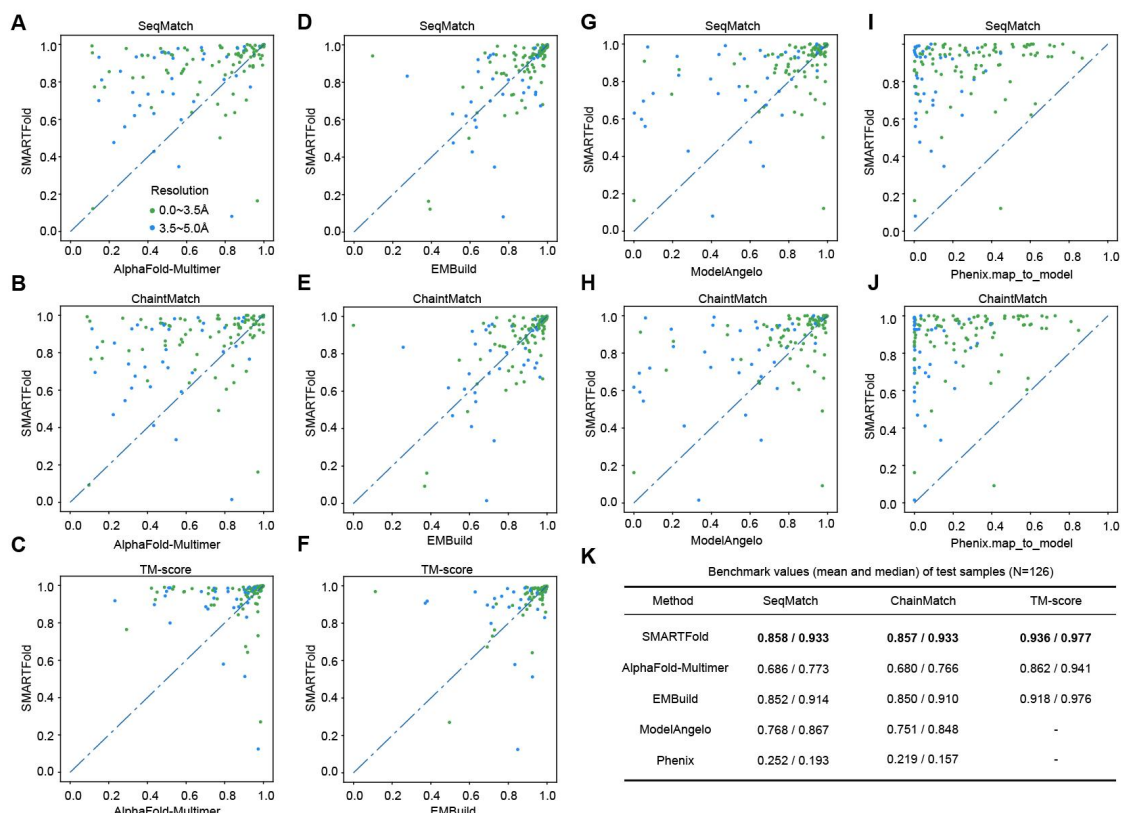


187

188 **Figure 4.** An example of multi-conformational monomer (PDB entries: 7via_G and 7vik_A). **(A)** The
189 deposited PDB model of 7via_G and 7vik_A are aligned using US-align (left). The segmented density
190 maps reflect two structure models well respectively (middle and right). **(B)** Model building results
191 from SMARTFold, AlphaFold2, EMBuild, ModelAngelo and Phenix.

192 **Evaluating built models against the high-resolution multi-chain dataset**

193 Next, we present our results on the multi-chain dataset, which consists of 126 multi-chain PDBs
194 with resolution $\leq 5\text{ Å}$. We compared our method with the aforementioned approaches, with the
195 exception of replacing AlphaFold2 with AlphaFold-Multimer. It can be seen in **Fig. 5** that
196 SMARTFold still achieved the highest scores in all metrics among all other methods (ChainMatch:
197 0.857 vs. 0.680, 0.850, 0.751, 0.219), even though EMBuild is very close to our method in
198 performance (ChainMatch: 0.865 vs. 0.850, TM-score: 0.936 vs. 0.918).



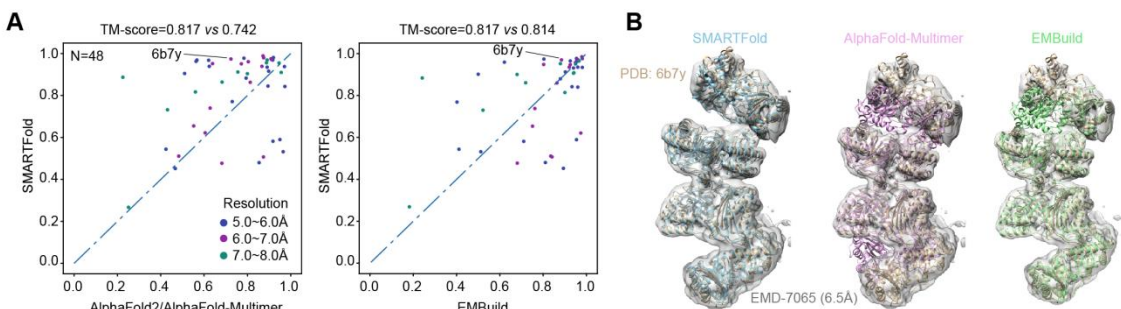
199

200

201 **Figure 5.** Comparison between SMARTFold, AlphaFold-Multimer, ModelAngelo and Phenix on 126
202 multimer dataset.

203 **Evaluating built models against the low-resolution dataset**

204 We further examined our performance on low-resolution PDBs. We assessed the above metrics on 48
205 PDB proteins with density map resolution worse than 5 Å. As expected, we observed a decline in
206 metrics as map resolution gets worse, like all other approaches do. Our method achieved a median
207 TM-score of 0.901 and a mean TM-score of 0.817 on these 48 proteins. **Fig. 6** reveals that
208 SMARTFold performed comparably to the state-of-the-art EMBuild method on low resolution dataset
209 and was better than AlphaFold2 / AlphaFold-Multimer. Since ModelAngelo was trained on high
210 resolution data only, we did not compare with it here.



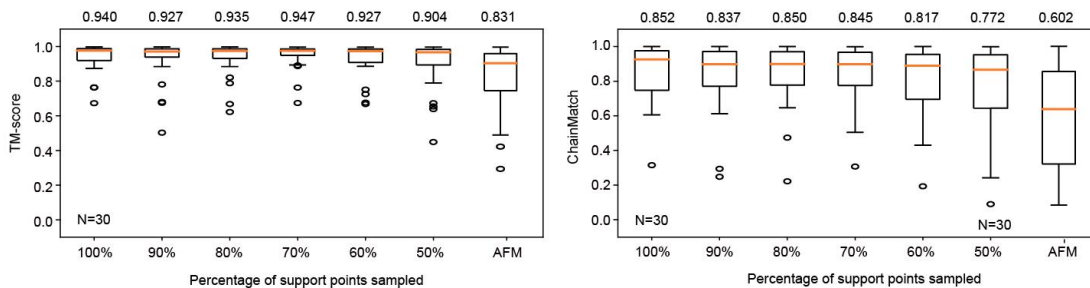
211

212 **Figure 6.** Comparison between SMARTFold, EMBuild and AlphaFold2/AlphaFold-Multimer on 48

213 low-resolution dataset.

214 **Robustness of the model on the number of support points**

215 For all the tests above, we set the number of support points sampled as the total length of the input
216 sequences. In order to test whether SMARTFold can use fewer support points to achieve comparable
217 performance, we conducted an experiment with 30 randomly selected samples from the multi-chain
218 dataset, and run SMARTFold for 5 times with 90%, 80%, 70%, 60%, and 50% support points (with
219 respect to the total sequence length) respectively. The results are shown in **Fig. 7**. We found that as
220 long as the number of sampled support points is greater than 70% of the sequence length, the
221 performance remains largely unaffected. Even when only 50% of the points are sampled, our method
222 still performs much better than AlphaFold-Multimer (TM-score: 0.904 vs 0.831). Thus, we can
223 conclude that our method is robust to the number of support points. Reducing the number of support
224 points not only saves runtime, but also reduces memory consumption.



225

226 **Figure 7:** TM-score and ChainMatch of SMARTFold using different sample rate of support points on
227 30 randomly selected multi-chain samples. AFM is the abbreviation of AlphaFold-Multimer.

228 **Point-residue distogram head**

229 To further encourage the model to learn the relationship between support points and residues, we
230 introduce a point-residue distogram head after the embedding module (EMformer) as an auxiliary task
231 of our model. This head takes the updated point-residue pair representation as input and predicts the
232 distance between each support point and residue (**Fig. 8A**). During training, the true distance labels
233 can be calculated prior to the loss computation and it is discretized to 10 bins. We employ a linear
234 layer to transform the input into logits and then utilize cross entropy loss for training. We use
235 unevenly spaced bins and different class weights to address the problem of imbalance data. Detailed
236 information can be found in **SI 6.2**.

237 The point-residue distogram head is found to be essential for the model to learn how to fold the
238 structure according to the positions of support points. Therefore it is of great help to improve the
239 overall model performance. On the other hand, this head also helps us know why our model works and
240 to prove that our model successfully absorbs the backbone information offered by the input density
241 map.

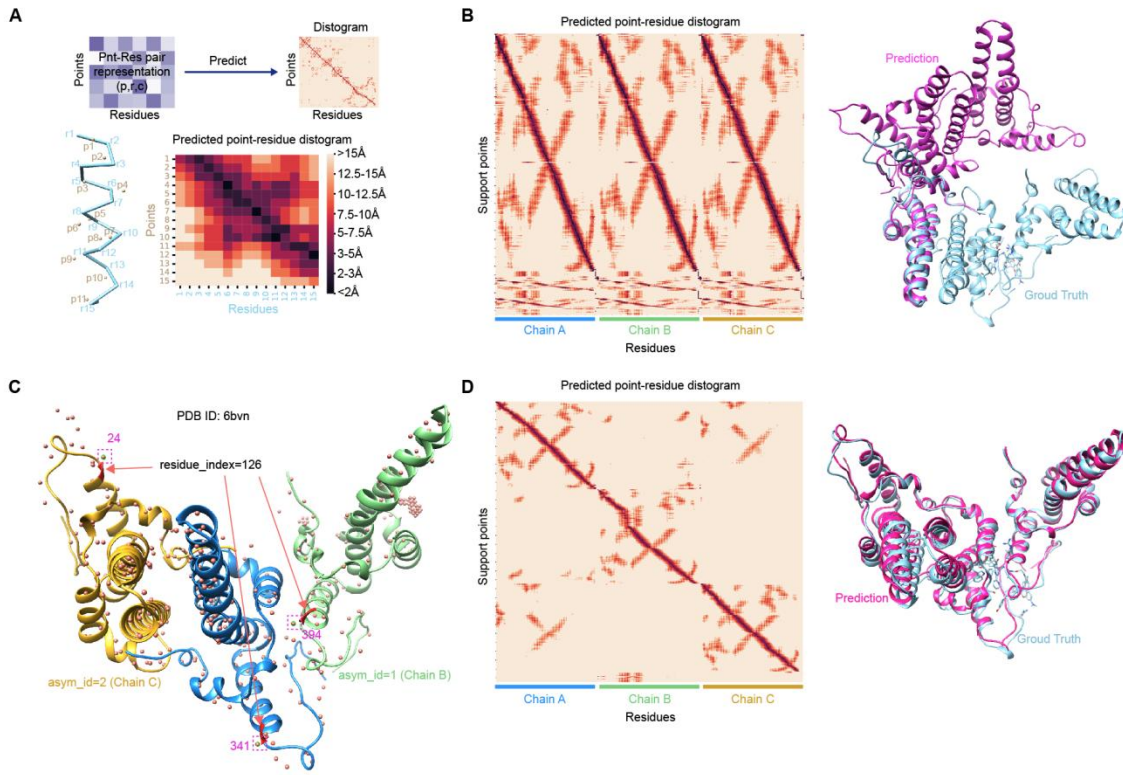
242 To demonstrate this, we visualized the output of point-residue distogram head as a heatmap. The

243 heatmap tells us the predicted correspondence between each point and residue. **Fig. 8A** shows an
244 example of the predicted distances between points and residues. All support points clearly find their
245 closest residues that should attend to. For example, point 3 is closest to residue 5 and the heatmap
246 shows that the distance between point 3 and residue 5 is very close ($< 2\text{\AA}$). This figure highlights that
247 although the support points do not necessarily fall on the actual positions of main chain atoms, their
248 distribution in the 3D space can effectively guide the model in discerning the backbone contour of the
249 protein chains. This explains how our model determines atom positions according to the input points.

250 **Importance of point-residue affinity**

251 Stoichiometry must be accounted for when predicting homogenous multimer structures. In the
252 prediction of a homodimerization, both ordering of two chain copies are equally valid, regardless of
253 their ordering in the ground truth model. We originally only used AlphaFold-Multimer's multi-chain
254 permutation alignment strategy (Evans et al., 2022) to solve the problem, but we found it unstable for
255 point-residue distogram loss. Thereby, we introduce a new feature called point residue affinity to
256 make the unconditional prediction (regarding which homogenous chain corresponds to which copy of
257 support points) to be a conditional one. The point residue affinity map $\text{affinity} \in \mathbb{R}^{p \times r}$ is a binary
258 matrix and each entry $\text{affinity}[i, j]$ indicates whether the point i is close to ($< 5\text{\AA}$) residue j .
259 Starting from the second recycle, the affinity is linear transformed and element-wise added to
260 point-residue representation. The point residue affinity map is only used in homogenous multimer
261 prediction, otherwise is set to all 0. For more detailed information, please refer to **SI 7**. **Fig. 8B-E**
262 provides an example of how point residue affinity features affect the homo-multimer structure
263 prediction.

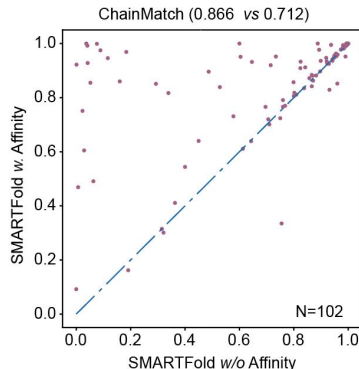
264



265

266 **Figure 8.** Point residue distance prediction and the use of point residue affinity feature to address the
267 ambiguity problem of homo-multimers. We take PDB 7bvn (a homogenous trimer) as an example
268 here (B-E). (A) An example of predicted point-residue distance diagram from point distogram head.
269 The predicted distances are discretized into 10 categories, where darker colors indicate closer
270 distances. (B) In the absence of point residue affinity feature, the predicted point-residue distance
271 map shows that each support point corresponds to 3 residue positions because there are 3 chain copies,
272 and the predicted structural model fails to align accurately with the ground truth model. (C) Using the
273 position of points and residues to construct the point residue affinity feature. Specifically, three entries
274 ([340, 126], [393, 276], [23, 426]) in the affinity feature are set to one. (D) The predicted distance
275 distogram after the affinity feature is set. Now each support point corresponds to a single residue
276 position respectively, and the predicted model can be well aligned with the ground truth model.

277 We found that when the affinity features are not used in inference, the result become much worse (Fig.
278 9).



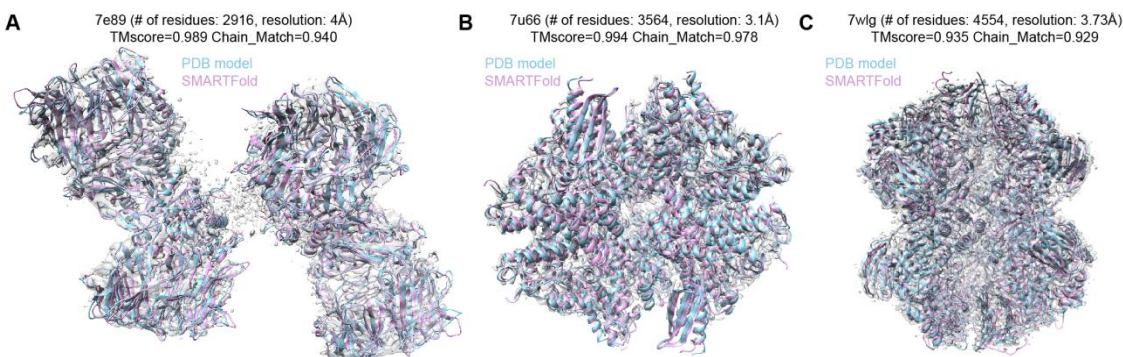
279

280 **Figure 9.** ChainMatch of SMARTFold with or without point residue affinity features in inference on
281 102 homomultimer samples.

282 **Long sequence inference**

283 Due to memory issues, our multimer model can only solve protein sequences with limited residue
284 length (up to 2500 residues on an A100, 40GiB GPU). For longer proteins, we offer an alternative
285 “single chain model” to tackle the memory problem. This version allows us to infer the whole
286 structure on a per-chain basis. This specially finetuned single chain model may take one chain
287 sequence as input while using the entire density map for sampling support points, though a lower
288 sampling rate (e.g, 50% of the whole sequence) would be applied. The whole inference process can be
289 completed by splitting the structure into individual chains and processing them separately, followed
290 by combining the results to obtain the final predicted structure. For more training and inference details
291 about this model, refer to **SI 10**.

292 **Fig. 10** illustrates three examples of long sequence protein prediction using single chain model: 7e89
293 (2916 residues), 7u66 (3564 residues) and 7wfg (4554 residues). TM-score on these samples are 0.989,
294 0.994 and 0.935 respectively. These examples show that our approach is capable of solving protein
295 structures with long sequences.



296

297 **Figure 10.** Long sequence inference samples with single-chain model. For all the three cases, the
298 predicted models (pink) are very close the deposited PDB structures (blue).

299 **Discussion**

300 In this study, we have proposed SMARTFold, an innovative end-to-end protein folding method by
301 integrating MSA and Cryo-EM maps. Our results have demonstrated that SMARTFold could
302 effectively build 3D protein structures model and output more accurate atomic positions compared
303 with previous state-of-the-art methods in single-chain and multi-chain benchmark dataset.
304 SMARTFold integrates experimental information by sampling support points from backbone
305 confidence map.

306 Although SMARTFold has demonstrated superior performance on the benchmark dataset, it still has
307 some limitations that need to be improved.

308 **Memory Cost & long sequence issue.** Due to the large amount of memory intensive operations, our
309 model only supports sequence length up to 2500 on 40GiB A100 GPU. There are some techniques for
310 making long sequence predictions. One way is to use unified virtual memory (UVM) of CUDA to
311 share memory space between GPU and host, keeping memory from overflow at the expense of more
312 running time. Another option is to use our alternative single chain model, to finish the inference by
313 chain. We plan to present a smaller model which has less layers and smaller feature channels to save
314 memory use.

315 **Time consumption.** Our model typically takes as much time as AlphaFold2 to run the inference, or
316 slightly higher due to support point relative calculations. Furthermore, MSA searching cost a
317 nonnegligible time in the whole procedure. One potential way to alleviate this is to replace MSA with
318 a protein language model. We leave this for future work as well.

319

320 **References**

321 Baek, M., DiMaio, F., Anishchenko, I., Dauparas, J., Ovchinnikov, S., Lee, G.R., Wang, J., Cong, Q.,
322 Kinch, L.N., Schaeffer, R.D., *et al.* (2021). Accurate prediction of protein structures and interactions using
323 a three-track neural network. *Science* *373*, 871-876.

324 Chen, M., and Ludtke, S.J. (2021). Deep learning-based mixed-dimensional Gaussian mixture model for
325 characterizing variability in cryo-EM. *Nat Methods* *18*, 930-936.

326 Evans, R., O'Neill, M., Pritzel, A., Antropova, N., Senior, A., Green, T., Žídek, A., Bates, R., Blackwell, S.,
327 Yim, J., *et al.* (2022). Protein complex prediction with AlphaFold-Multimer. *bioRxiv*,
328 2021.2010.2004.463034.

329 He, J., Lin, P., Chen, J., Cao, H., and Huang, S.Y. (2022). Model building of protein complexes from
330 intermediate-resolution cryo-EM maps with deep learning-guided automatic assembly. *Nat Commun* *13*,
331 4066.

332 Jamali, K., Kimanis, D., and Scheres, S.H.W. (2022). A graph neural network approach to automated
333 model building in cryo-EM maps, pp. arXiv:2210.00006.

334 Jumper, J., Evans, R., Pritzel, A., Green, T., Figurnov, M., Ronneberger, O., Tunyasuvunakool, K., Bates,
335 R., Zidek, A., Potapenko, A., *et al.* (2021). Highly accurate protein structure prediction with AlphaFold.
336 *Nature* *596*, 583-589.

337 Nakane, T., Kotecha, A., Sente, A., McMullan, G., Masiulis, S., Brown, P., Grigoras, I.T., Malinauskaitė,
338 L., Malinauskas, T., Miehling, J., *et al.* (2020). Single-particle cryo-EM at atomic resolution. *Nature* *587*,
339 152-156.

340 Pfab, J., Phan, N.M., and Si, D. (2021). DeepTracer for fast de novo cryo-EM protein structure modeling
341 and special studies on CoV-related complexes. *Proc Natl Acad Sci U S A* *118*.

342 Punjani, A., Rubinstein, J.L., Fleet, D.J., and Brubaker, M.A. (2017). cryoSPARC: algorithms for rapid
343 unsupervised cryo-EM structure determination. *Nat Methods* *14*, 290-296.

344 Ronneberger, O., Fischer, P., and Brox, T. (2015). U-Net: Convolutional Networks for Biomedical Image
345 Segmentation, pp. arXiv:1505.04597.

346 Scheres, S.H. (2012). RELION: implementation of a Bayesian approach to cryo-EM structure
347 determination. *J Struct Biol* *180*, 519-530.

348 Terashi, G., and Kihara, D. (2018). De novo main-chain modeling for EM maps using MAINMAST. *Nat
349 Commun* *9*, 1618.

350 Terwilliger, T.C., Adams, P.D., Afonine, P.V., and Sobolev, O.V. (2018). A fully automatic method
351 yielding initial models from high-resolution cryo-electron microscopy maps. *Nat Methods* *15*, 905-908.

352 Wang, C., Zeng, J., and Wang, J. (2022). Structural basis of bacteriophage lambda capsid maturation.
353 *Structure* *30*, 637-645 e633.

354 Xu, J. (2019). Distance-based protein folding powered by deep learning. *Proc Natl Acad Sci U S A* *116*,
355 16856-16865.

356 Yip, K.M., Fischer, N., Paknia, E., Chari, A., and Stark, H. (2020). Atomic-resolution protein structure
357 determination by cryo-EM. *Nature* *587*, 157-161.

358 Zhang, C., Shine, M., Pyle, A.M., and Zhang, Y. (2022). US-align: universal structure alignments of
359 proteins, nucleic acids, and macromolecular complexes. *Nat Methods* *19*, 1109-1115.

360 Zhang, Y., and Skolnick, J. (2004). Scoring function for automated assessment of protein structure template
361 quality. *Proteins* *57*, 702-710.

362 Zhong, E.D., Bepler, T., Berger, B., and Davis, J.H. (2021). CryoDRGN: reconstruction of heterogeneous
363 cryo-EM structures using neural networks. *Nat Methods* *18*, 176-185.

364

365 **Acknowledgments**

366 We thank colleagues from Cryo-EM Center of Shuimu BioSciences for their advices for SMARTFold
367 on internal dataset. We thank Zhenqian Guo from Shuimu BioSciences for his kind help and
368 maintenance of computing infrastructure. **Funding:** This research was funded by Shuimu
369 BioSciences.

370 **Author contributions**

371 P.L., L.G. and H.L. conceived the idea, implemented the method, carried out the experiments and
372 wrote the manuscript. P.L. collected and processed the data with the help of B.L. F.M. and X.N.
373 benchmarked the model using internal dataset and proposed the useful advices. C.G. supervised the
374 project and modified the manuscript.

375 **Competing interests**

376 The novel aspects of the method have been described in a patent application filed by the authors.

377